BULLETIN OF THE POLISH ACADEMY OF SCIENCES
TECHNICAL SCIENCES, Vol. 70(5), 2022, Article number: e141723
DOI: 10.24425/bpasts.2022.141723

Study of rock fracture under blast loading

Paweł BARANOWSKI[1]*, **Michał KUCEWICZ**[1], **Mateusz PYTLIK**[2], **and Jerzy MAŁACHOWSKI**[1]

[1] Military University of Technology, Faculty of Mechanical Engineering, Institute of Mechanics & Computational Engineering, ul. Gen. S. Kaliskiego 2, 00-908 Warsaw, Poland

[2] Central Mining Institute, Conformity Assessment Body, 40-166 Katowice, Poland

Abstract. A study of dolomite rock material failure using a simple small-scale blast setup is presented. Laboratory tests were conducted using disc specimens drilled with a borehole in the center. A detonation cord and a blasting cap were fitted inside the borehole to induce cracking and fracturing of the specimens. The specimens were inserted between two steel plates, which were compressed against the specimen using bolt screws. Prior to testing, the most suitable screw torque for constraining the vertical displacement of the specimen surfaces without compressing the specimen was selected based on numerical simulations. Then, the experimental tests with the blasting cap were simulated using the Johnson–Holmquist II (JH-2) material model, and the properties of the blasting cap were determined and verified in two special tests with a lead specimen. Possessing the validated model, the influence of specimen thickness on the cracking patterns was finally analyzed. This paper presents a relatively easy method for studying rock material behavior under blast loading and for validating the numerical and constitutive models used for rock simulations.

Key words: Johnson–Holmquist II model (JH-2); rock; blasting; fracture; small-scale testing.

1. INTRODUCTION

High explosive (HE) materials are commonly used in civil engineering and mining. The detonation of HE materials in rock provides a sudden release of energy, which generates a shock wave that propagates through the rock. Ultimately, cracking and fragmentation of the rock occur, which are desired phenomena when excavating minerals from rocks. Blasting and HE interactions with rock or other brittle materials are challenging but important topics of research. Numerous experimental and numerical studies of varying scales have been conducted to understand these complicated phenomena including blasting and material [1–9]. However, large-scale and field tests are relatively costly and difficult to conduct. Consequently, small-scale laboratory experiments are often used to study the failure of various materials subjected to strongly dynamic loading resulting from HE detonation [10–18]. Most recent laboratory-scale blasting studies have focused on fracture patterns and crack propagation in granite rock [14–16, 19–22] or concrete [10, 12, 23, 24], although a recent paper by Jeong H. *et al.* [25] presented experimental and numerical tests of cylindrical specimens of polymethyl methacrylate (PMMA).

Experimental tests of small-scale blasting are frequently coupled with numerical simulations using various methods and techniques. For instance, the 3D multi-material arbitrary Lagrangian-Eulerian (MM-ALE) formulation method has proved effective in numerous engineering problems and has also been implemented to study rock blasting [16, 19–22]. This method develops models using finite elements (FEs), and the interaction between the HE and other non-Lagrangian bodies is simulated as fluid-structure interaction (FSI). In [15], a fully meshless approach was utilized, and a whole model was represented using smoothed particle hydrodynamics (SPH); the results were validated using outcomes from [14]. A peridynamics-based numerical approach was successfully used in [26].

Regardless of the method used to numerically reproduce blasting and rock failure, all simulations require a reliable material model. Several constitutive models that simulate the behavior of rock and brittle materials very effectively are found in hydrodynamics computer code (hydrocode) libraries. The most important of these models are the Johnson–Holmquist II (JH-2) model [14, 27, 29, 29–34], the Holmquist–Johnson–Cook model (Johnson–Holmquist Concrete model – JHC model) [35–38], the Riedel–Hiermaier–Thoma (RHT) model [39, 40], the Continuous Surface Cap (CAP) model [41, 42] and the Karagozian and Case Concrete (KCC) model [43–46].

The main aim of the present paper is to study a shock-induced fracture of rock material using a simple small-scale blasting laboratory setup and detailed numerical modeling. The objective was to design small-scale tests that are not only as simple as possible to carry out but also provide better insights into crack propagation and fracture patterns in laboratory-scale rock material specimens under blast loading. This study is a continuation of previous works [32, 37, 43, 47] in which dolomite was subjected to experimental testing, constitutive modeling, and numerical simulations of blasting. Other researchers conducted a similar analysis of sandstone with a sin-

*e-mail: pawel.baranowski@wat.edu.pl

Manuscript 2022-05-10, revised 2022-06-28, initially accepted for publication 2022-07-17, published in October 2022.

gle pre-crack [48]. The authors of the present study also previously conducted small-scale blasting tests using cylindrical dolomite specimens. [49], which inspired further investigations to design and propose an even easier test for testing rock materials loaded with explosive waves. In the present paper, disc specimens of dolomite with a central hole were placed between two steel plates to achieve quasi-plane strain conditions. Two types of detonation sources were used in the central borehole: a detonation cord with hexogen (RDX) covered with a lead sheath or a blasting cap. The use of a blasting cap as the detonation source provided more reproducible results, and thus the blasting cap was considered in the subsequent numerical analysis. The properties of the blasting cap were also evaluated by analyzing hole expansion in two tests with lead cylindrical specimens. The properties of the HE material were determined in numerical simulations and verified using the results of the experimental tests. Prior to testing, the most suitable screw torque for constraining the vertical displacement of the specimen surfaces without compressing the specimen was selected based on numerical simulations. Ultimately, numerical tests simulating the laboratory blasting experiment were performed to further analyze the cracking and fracture characteristics of the dolomite specimen, including the influence of specimen thickness on the cracking patterns. This study provides a useful complement to a large number of rock blasting papers, and the method described here can be effectively adopted to determine and validate the constitutive models JH-2 parameters for rock or concrete.

2. MOTIVATION

The main aim of previous studies combining small-scale blasting tests with numerical simulations, e.g. [49] was to analyze the shock-induced fracture of rock and other brittle materials. Cracking characteristics are typically analyzed within the surface perpendicular to the axis of the borehole, primarily due to the significant difference between the compressive strength and tensile strength of rock. Previous work has shown that HE combustion through the axis of the borehole results in spalling and scabbing fractures as well as vertical crack propagation. Ultimately, HE combustion through the borehole axis can influence fractures in the bottom or top surface of the specimen but analyzing the cracking characteristics only on those surfaces may not be sufficient for comparison with other similar studies. Moreover, the complexity of the test and natural imperfections of rock (joints, micro- and macro-cracks) may make it difficult to obtain repeatable results. Consequently, a simple method is needed for analyzing specimen cracking patterns without a complicated experimental setup.

The main assumption in developing this method was to consider a quasi-2D problem corresponding to the cross-section of the middle of a 3D specimen, where the influence of the stress wave reflections from the top and bottom surfaces is the smallest. To confirm the presence of quasi-2D conditions, a new model was prepared using a slice of the whole 3D dolomite specimen presented in [49]. The initial boundary conditions were nearly identical to those used for the whole specimen, and the appropriate displacement of the hexagonal element faces (representing the FE model of the specimen) perpendicular to the axis of the HE was fixed using symmetry (Fig. 1). This approach represented an initial attempt to determine whether quasi-2D models could be used to simply and rapidly model large-scale blasting to optimize underground blasting techniques.

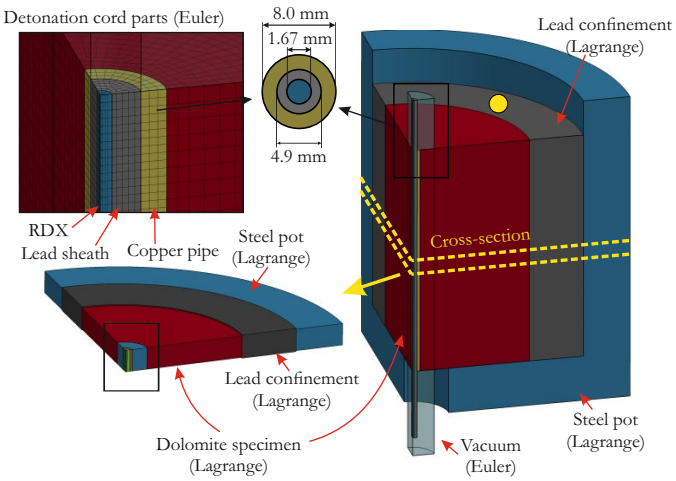

Fig. 1. The quasi-2D numerical model acquired from the cross-section of the full 3D model of the small-scale blasting test of dolomite rock

Figure 2 presents the cracking patterns of the middle cross-section of the 3D numerical model and of the quasi-2D model, which was cut from the 3D model with the appropriate boundary conditions. Both models give nearly identical cracking patterns, with 20 radial cracks. Some small discrepancies are apparent in the vicinity of the borehole and cracking placement. The crushing zones are identical, which indicates that the quasi-2D model does not excessively stiffen the rock despite blocking perpendicular deformation of the specimen surfaces. These results confirmed the advisability of developing a suitable experimental setup for such investigations under quasi-plane strain conditions.

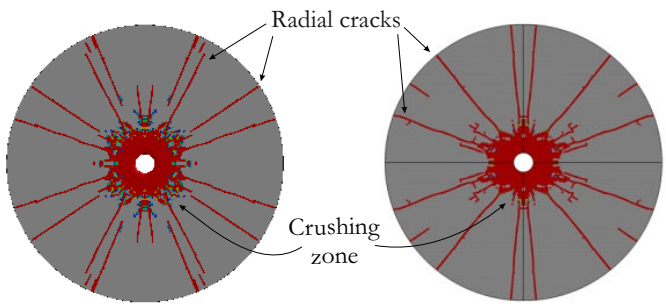

Fig. 2. Comparison of the blast-induced crack patterns obtained from the full 3D numerical model and quasi-2D numerical model

3. EXPERIMENTAL TEST CONFIGURATION

Four disc-shaped specimens of dolomite were used in the experiment. Each specimen was placed between two steel plates to achieve quasi-plane strain conditions. The steel plates were joined using eight screw bolts placed around the specimen. The steel plates were not tightly connected. Prior to testing, the torque of the bolt screws was adjusted according to the numerical model and prestress of the bolt screws to ensure that the steel plates did not compress the specimen significantly (maximum Z stress of 1.0 MPa) but mainly constrained the Z displacement of the specimen (see Section 5.1). Only strain in the X and Y directions was considered. Furthermore, the specimen was loosely held using a clamp to prevent extensive failure of the specimen. Each specimen had a diameter of 130 mm and a height of 15 mm. In the first round of experiments, a detonation cord composed of RDX material covered with a lead sheath was placed inside the borehole, which had a diameter of 5.0 mm. The outer diameter of the cord was 4.90 mm, and the diameter of the RDX core was 1.67 mm. The average detonation velocity (D) measured by the electronic probes was 4840.0 m/s. The outcomes were not satisfactory (please see Section 5.2 for further discussion), and the detonation cord was replaced with a blasting cap in the next round of experiments. Identical dolomite specimens were used, but the diameter of the borehole was increased to 7.0 mm to accommodate the blasting cap. The blasting cap consisted of a zinc shell with a length of 41.0 mm, the wall thickness of 0.2 mm, and the bottom thickness of 0.65 mm. The HE comprised 300 mg of a mixture of lead azide and lead trinitroresorcinate pressed to a volume density of 1600.0 kg/m^3 and was loaded in the bottom of the cap. Simple schematics of the experiments, detonation cord, and blasting cap are presented in Fig. 3.

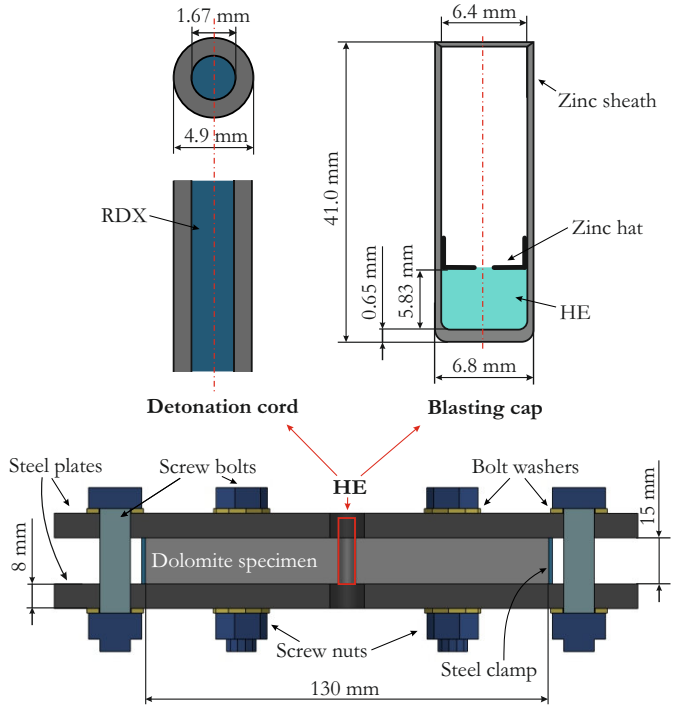

Fig. 3. Schematics of the experimental set-up, detonation cord, and blasting cap

4. NUMERICAL MODELING

4.1. Model definition

Following the experimental tests, numerical simulations were conducted. For all analyses, an explicit integration procedure with massively parallel processing (MPP) LS-Dyna code was adopted. The blasting process and all necessary interactions were simulated using the MM-ALE algorithm. Since the simulated problem is symmetric, a quarter of the model was developed with the appropriate conditions applied where necessary. Importantly, using a quarter model of the specimen does not affect the propagation of cracks at the symmetry planes of the model. The central part of the dolomite specimen was embedded in the Eulerian air domain. A non-reflecting boundary was applied on its outer surfaces to consider the flow of the pressure outside the air domain. Thus, all parts of the blasting cap were treated as Eulerian parts, whereas Lagrangian elements (brick FEs) with one integration point were used to model the dolomite specimen. The fluid-structure interaction between the blasting cap parts and the dolomite specimen was defined using a penalty-based contact procedure [50]. The dolomite specimen described with the JH-2 model (the parameters are shown in Table 1) was represented using a 0.5 mm mesh. By contrast, an element size of 0.07 mm to 0.14 mm was considered in the Eulerian domain, where the coupling with the Lagrangian dolomite specimen occurred. The steel plates and clamp were represented using solid elements with an average size of 1.0 mm. The screws, nuts, and washers were modeled using solid elements (FE sizes from 1.5 mm to 3.0 mm). In total, the model consisted of 739,755 elements.

The steel clamp and steel plates were described using an elastic material model with the following properties: $E_{\text{steel}} = 210.0$ GPa, $\rho_{\text{steel}} = 7850.0$ kg/m^3, and $\nu_{\text{steel}} = 0.3$. The elasto-plastic material model for the screws, nuts, and washers considered the same elastic properties used for the clamp and plates with a yield stress of $R_e = 800.0$ MPa and tangent modulus of $E_{\text{tan}} = 1010.0$ MPa. The zinc sheath of the blasting cap was modeled using the Johnson–Cook (JC) constitutive model. Since parameters for pure zinc are not available in the literature, the parameters for copper adjusted for the density of zinc were used instead (Table 2). The high explosive burn (HEB) constitutive model with the Jones–Wilkins–Lee (JWL) equation of state (EOS) was used to describe the HE and its detonation products. The properties of the HE in the blasting cap were correlated and validated in two additional tests (see Section 4.1), and the final parameters are listed in Table 3. Air was considered a simple ideal gas with vacuum properties.

The discussed numerical model (Fig. 4) was used to simulate the following cases:

- Case #1: The influence of the bolt screw torque and consequently bolt preload [51, 52] was analyzed, and the most suitable value ensured that the steel plates only constrained the vertical displacement of the specimen surfaces and did not compress the specimen too much was selected for use in the experimental tests. Several different torque values were considered, and six tests were selected for presentation and analysis: 0.5 Nm, 1.0 Nm, 2.0 Nm, 3.0 Nm, 4.0 Nm, and 5.0 Nm. The numerical simulations were conducted with

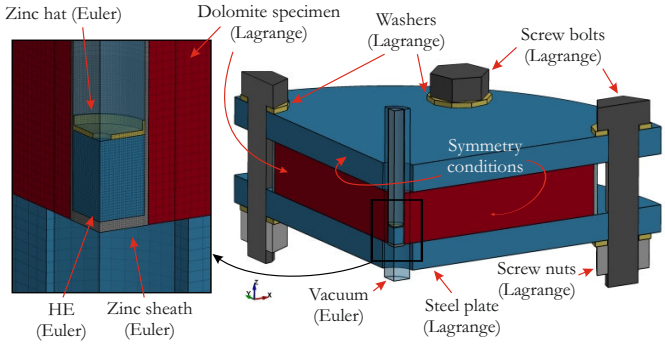

Fig. 4. Numerical model of the small-scale blasting test of dolomite rock with a close-up view of the detonation cord and borehole

the dynamic relaxation phase only, and the preloading due to torquing of the bolt was considered.

- Case #2: The experiment was reproduced using a two-stage procedure to consider the initial bolt screw clamping: static preloading using dynamic relaxation with Lagrange parts only (stage #1) and dynamic blast loading with FSI (stage #2) to reproduce the actual laboratory test with the Eulerian domain. In stage #1, the selected torque from Case #1 was used. In stage #2, the results from the previous stage were used as a prestress field distributed in the screw bolts and other parts of the model.
- Case #3: The influence of specimen thickness on failure and cracking characteristics was analyzed. Having validated the numerical model, a parametric study was conducted with several different specimen thicknesses ranging from 6.0 mm to 15.0 mm. The specimen in the first analysis had a thickness similar to the height of the HE used in the blasting cap, whereas the last one corresponded to the experimental test and Case #2.

4.2. Constitutive modeling

Dolomite specimen

The behavior of dolomite was simulated using the JH-2 constitutive model with previously determined and verified parameters [32], which are presented in Table 1. Since the value of T representing the maximum hydrostatic tensile pressure is dependent on the FE size and the dolomite specimen was modeled using an average mesh size of 0.5 mm, $T = 70.0$ MPa was used in the simulations, according to the findings in [32]. The model is based on the relationship between normalized values of equivalent stress and pressure and is described by intact, damaged, and fractured surfaces. The normalized intact strength of the material presented can be described using the following formula [29, 31]:

$$\sigma_I^* = A\,(P^* + T^*)^N\,(1 + C \ln \dot{\varepsilon}^*)\,, \tag{1}$$

where $\sigma_I^* = \sigma_I/\sigma_{\mathrm{HEL}}$ is the normalized intact strength; σ_I is the current equivalent stress; σ_{HEL} is the equivalent stress at the Hugoniot elastic limit (HEL); $P^* = P/P_{\mathrm{HEL}}$ is the normalized hydrostatic pressure; P is the current hydrostatic pressure; $T^* = T/P_{\mathrm{HEL}}$ is the normalized maximum tensile hydrostatic pressure; $\dot{\varepsilon}^* = \dot{\varepsilon}/\dot{\varepsilon}_0$ is the dimensionless strain rate; $\dot{\varepsilon}$ is the current equivalent strain rate; and $\dot{\varepsilon}_0 = 1]\,\mathrm{s}^{-1}$ is the reference strain rate. The damage state σ_D^* is determined by [29, 31]:

$$\sigma_D^* = \sigma_I^* - D\,(\sigma_I^* - \sigma_F^*)\,, \tag{2}$$

where D is a damage factor (index) and takes a value between 0 (undamaged) and 1 (fully damaged).

The fractured surface σ_F^* of the material is described using the following formula [29, 31]:

$$\sigma_F^* = B\,(P^*)^M\,(1 + C \cdot \ln \dot{\varepsilon}^*)\,, \tag{3}$$

where B and M are the fractured material constants.

Table 1
Dolomite material properties of the JH-2 model [32, 47]

Parameter	Value	Unit
Density, ρ	2840.0	kg/m^3
Poisson's ratio, ν	0.24	–
Bulk modulus, K_1	30834.5	MPa
Shear modulus, G	19059.6	MPa
Young's modulus, E	47410.3	MPa
Hugoniot elastic limit, HEL	2750.0	MPa
HEL pressure, P_{HEL}	1945.0	MPa
Maximum tensile strength*, T	70.0	MPa
Intact strength coefficient, A	0.78	–
Fractured strength coefficient, B	0.65	–
Strain rate coefficient, C	0.02	–
Intact strength exponent, N	0.45	–
Fractured strength exponent, M	0.45	–
Bulk factor, β	1.0	–
Damage coefficient, D_1	0.001	–
Damage coefficient, D_2	1.15	–
Pressure coefficient 2, K_2	700000.0	MPa
Pressure coefficient 3, K_3	5650000.0	MPa
Maximum normalized fracture strength, $\sigma^*_{\max}$	0.35	–
Density, ρ	2840.0	kg/m^3
Poisson's ratio, ν	0.24	–

* Value adjusted based on mesh size in the model

Blasting cap

The blasting cap used in this study comprised an explosive material covered with a zinc sheath. The laboratory tests with the detonation cord and RDX HE were not considered in the numerical simulations (see Section 5.2). The zinc sheath and hat of the blasting cap were modeled using the JC model, which has been extensively adopted in numerous simulations of dynamic problems [53]. Parameters for pure zinc are not available in the

literature, and thus the parameters for copper adjusted for the density of zinc were considered instead (Table 2). The model provides a prediction of flow stress σ_{flow} for large strains and high strain rates and is given by the following relation [50]:

$$\sigma_{\text{flow}} = \left[A_{\text{JC}} + B_{\text{JC}}(\varepsilon^p)^{N_{\text{JC}}}\right](1 + C_{\text{JC}} \ln \dot{\varepsilon}_*^p) \left[1 - \left(\frac{T - T_{\text{rJC}}}{T_{\text{mJC}} - T_{\text{rJC}}}\right)^{M_{\text{JC}}}\right], \quad (4)$$

where ε_p is the equivalent plastic strain and $\dot{\varepsilon}_p$ is the equivalent plastic strain rate.

Table 2
Blasting cap sheath material properties of the JC model for copper [54–56]

Parameter	Value	Unit
Mass density*, ρ	7120.0	kg/m^3
Shear modulus, G	48.0	GPa
JC yield stress, A_{JC}	90.0	MPa
JC hardening parameter, B_{JC}	292.0	MPa
JC hardening parameter, N_{JC}	0.31	–
JC strain rate sensitivity parameter, C_{JC}	0.025	–
JC thermal softening parameter, M_{JC}	1.09	–
Specific heat, $C_{p\text{JC}}$	3.83×10^8	mJ/kgK
Reference strain rate, EPSO$_{\text{JC}}$	1.0	1/s
Reference temperature, $T_{r\text{JC}}$	293.0	K
Melting temperature, $T_{m\text{JC}}$	1356.0	K
JC failure parameter, D_1	0.54	–
JC failure parameter, D_2	4.89	–
JC failure parameter, D_3	3.03	–
JC failure parameter, D_4	0.014	–
JC failure parameter, D_5	1.12	–

* Value adjusted to be similar to zinc density

The HE and its detonation products were described using the HEB constitutive model with the JWL EOS:

$$p = A_{\text{HE}}\left(1 - \frac{\omega}{R_1 V_{\text{HE}}}\right)e^{-R_1 V_{\text{HE}}} + B_{\text{HE}}\left(1 - \frac{\omega}{R_2 V_{\text{HE}}}\right)e^{-R_2 V_{\text{HE}}} + \frac{\omega E_0}{V_{\text{HE}}}, \quad (5)$$

where $V_{\text{HE}} = \rho_{0\,\text{HE}}/\rho_{\text{HE}}$; $\rho_{0\,\text{HE}}$ is the initial density of the HE; ρ_{HE} is the actual density of the HE; E_0 is the detonation energy per unit volume and initial value of E of the HE; and A_{HE}, B_{HE}, R_1, R_2, and ω are empirical constants determined for a specific type of explosive material.

The initial parameters of the HE were obtained from the program EXPLO5. The volume density and average detonation velocity were equal to $\rho_{0\,\text{HE}} = 1600.0$ kg/m^3 and $D_{\text{HE}} = 2073.0$ m/s, respectively. The Chapman–Jouguet pressure p_{CJ} and initial energy E_0 were determined to be 1541.0 MPa and 1718.0 MPa, respectively.

In further studies, the HE properties of the blasting cap were correlated based on two tests using cylindrical lead specimens. In test No. 1, a specimen with a height of 15.0 mm and a diameter of 40.0 mm was used. Test No. 2 used a cylindrical lead specimen with a height of 60.0 mm and a diameter of 40.0 mm. In both specimens, a hole with a diameter of 7.0 mm was drilled in the center and fitted with a blasting cap. In test No. 1, the radial deformation of the lead specimen was investigated, whereas, in test No. 2, the final volume and dimensions of the borehole were analyzed. The geometric dimensions after the test, including the borehole and specimen diameters, were comprehensively measured.

Since significant deformation of the lead specimen occurred in both tests, a full Eulerian approach was adopted. Furthermore, 2D axisymmetric models were developed to speed up the numerical calculations. To simulate the behavior of the lead, the Modified Johnson–Cook constitutive model (MJC) was used with parameters taken from [57, 58]. The experimental setups are shown in Fig. 5a, and the corresponding numerical models are shown in Fig. 5b.

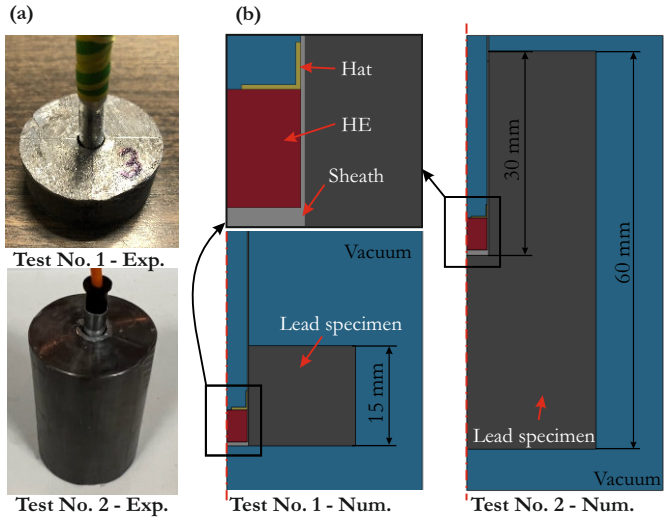

Fig. 5. Testing of the blasting cap properties: (a) experiments and (b) numerical models

The values of R_1, ω and E_0 in the JWL EOS (equation (5)) were iteratively changed until the final deformations of the specimens in the numerical simulations were sufficiently consistent with real-world tests. The final values were $R_1 = 4.59$, $\omega = 0.34$ and $E_0 = 2718.0$ MPa. Table 3 presents the final HEB and EOS parameters that gave the best correlation with the real-world tests (Fig. 6).

A remarkably close agreement between the numerical and experimental results was obtained in both tests, confirming that the HEB material model with the JWL EOS correctly described the blasting cap. Table 4 compares the numerical and experimental results. The maximum deviation, 6.5%, occurred in the measured final volume of the borehole in test No. 2.

Table 3
HE material properties of the HEB model with the JWL EOS

Parameter	Value	Unit
Initial density, ρ_{0HE}	1601.0	kg/m^3
Detonation velocity, D	2091.0	m/s
Chapman–Jouguet pressure, p_{CJ}	1541.0	MPa
Empirical constant, A_{HE}	24483.1	MPa
Empirical constant, B_{HE}	582.9	MPa
Empirical constant*, R_1	4.59	–
Empirical constant, R_2	1.37	–
Empirical constant*, ω	0.34	–
Detonation energy per unit volume*, E_0	2.718	J/mm^3

* Initial values were modified during correlation tests

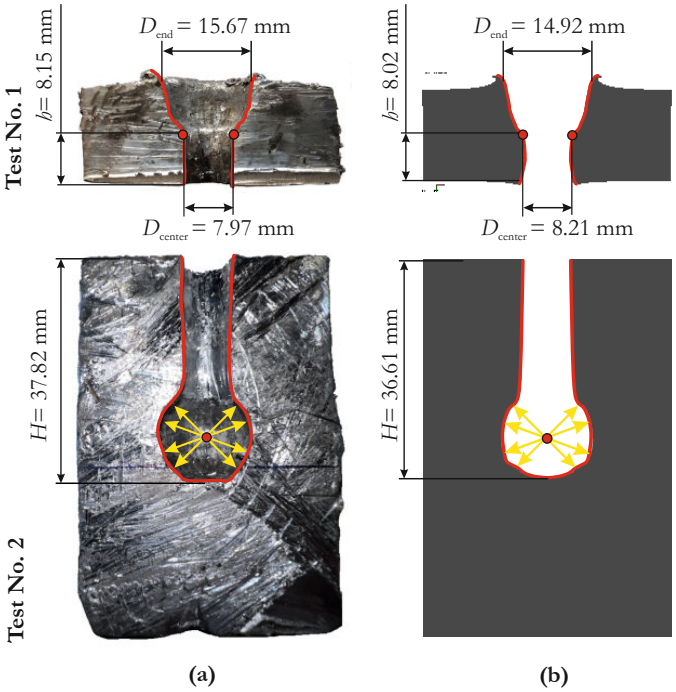

Fig. 6. Comparison of lead specimen deformation after blasting cap expansion: (a) experiment; (b) numerical simulation; (c) numerical simulation: plastic strain distribution

5. RESULTS AND DISCUSSION

5.1. Analysis of the screw bolt torque

Prior to experimental testing, the correct torque of the screws was determined using the developed numerical model. The main intent of this stage was to determine the conditions that would allow the experimental tests to be performed under quasi-plane-strain conditions. For each case with a different torque value, the pressure distribution was analyzed and compared with other simulations. In Fig. 7, pressure maps are presented for all six cases. The pressure fringe was manually constrained from -1.0 MPa to $+1.0$ MPa. Increasing the torque of the screw bolts resulted in a non-uniform distribution of the pressure within the specimen. The larger the torque, the larger the difference in the pressure value within the dolomite volume. In the first two cases, the distribution was nearly uniform, and the case with a torque value of 1.0 Nm was most appropriate since the specimen was not compressed significantly and had the most uniform pressure distribution over the specimen thickness. Since the main intention of the steel plates was to prevent the sample from moving along the Z axis, a torque value of 1 Nm was selected for further use in the experimental tests. Increasing the torque resulted in larger nonuniformity, and the concentrations of the maximum pressure were largest when the torque was 5.0 Nm in the last case.

Table 4
Comparison of lead specimen deformation obtained from the simulation and experiment (tests No. 1 and No. 2)

	Compared data	Experiment	Simulation	Error (%)
Test No. 1	Beginning of expansion, h (mm)	8.15	8.02	1.6
	Hole end diameter, D_{end} (mm)	15.67	14.92	4.8
	Hole central part diameter, D_{center} (mm)	7.97	8.21	3.0
Test No. 2	Bottom of the hole, H (mm)	37.82	36.61	3.2
	Average hole diameter, D_{av} (mm)	14.71	14.38	2.3
	Final volume, V (mm^3)	1663.2	1556.9	6.5

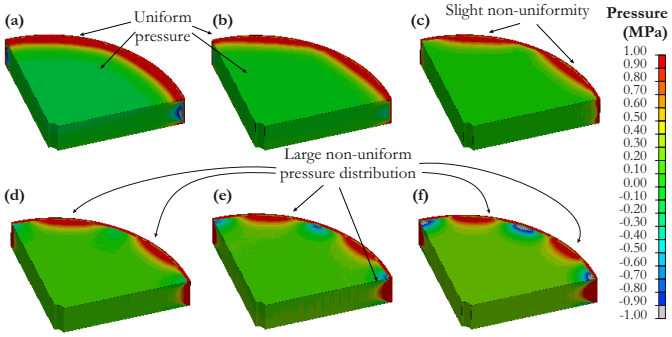

Fig. 7. Comparison of pressure distribution in the specimen after torquing of the screw bolts: (a) 0.5 Nm, (b) 1.0 Nm, (c) 2.0 Nm, (d) 3.0 Nm, (e) 4.0 Nm, and (f) 5.0 Nm

5.2. Small-scale blast tests

Experimental results

Exemplary specimen failure patterns for the detonation cord and blasting cap are presented in Fig. 8. Previous studies revealed a strong heterogeneous structure of dolomite as well as pre-cracking inside dolomite specimens [37, 43]. In addition, pores and inclusions varying in size from 1.0 mm to 10.0 mm were observed. These imperfections impact the brittle behavior of the dolomite and make it challenging to obtain reproducible results under identical test conditions.

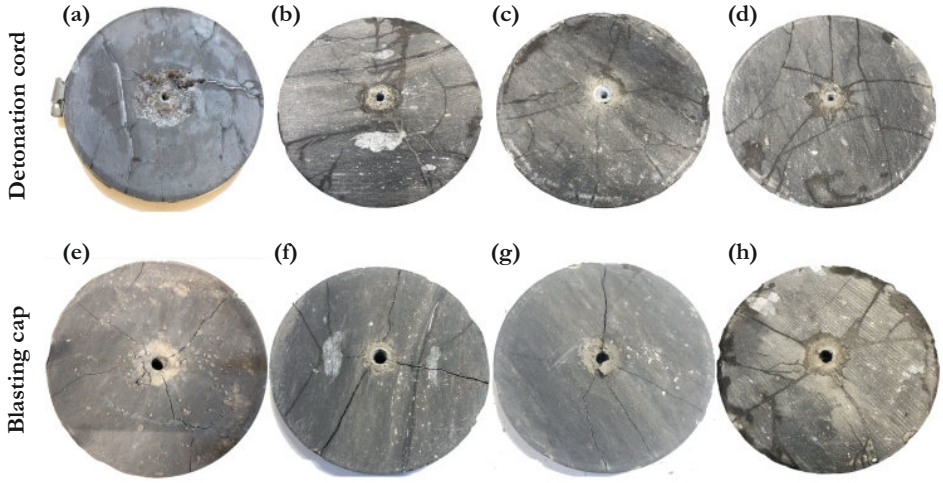

Fig. 8. Failure of exemplary dolomite specimens after experimental small-scale blasting tests: (a) Specimen No. 1, (b) Specimen No. 2, (c) Specimen No. 3, (d) Specimen No. 4, (e) Specimen No. 5, (f) Specimen No. 6, (f) Specimen No. 7, (f) Specimen No. 8

For the tests with the detonation cord, four dolomite specimens were studied, and different outcomes were observed for each test. There may be several reasons for such discrepancies, including a heterogenous dolomite structure with the mentioned imperfections. Furthermore, all tested specimens were cut from the cylindrical rock cores with a length close to 1.0 m. Several pre-cracks along the rock core length were observed and differences between the rock structure may have occurred. Therefore, specimens No. 1 to 4 could have slightly different properties and structures compared to the specimens tested with the blasting cap (specimens No. 5–8). Specimen No. 1 exhibited an extensive crushing zone around the borehole, in contrast to the other three specimens. In all cases, a fracture zone consisting of mainly radial cracks was visible. However, the fracture intensity in this zone differed among the specimens. A strong influence of the mentioned imperfections, which resulted in transverse cracking, was observed and was most evident in Specimen No. 4. It was difficult to evaluate the number of cracks in Specimen No. 1, and Specimen No. 3 exhibited the largest number of cracks. The cracking characteristics of the latter specimen were most consistent with those of shock-induced blasting of rock, with a clearly visible crushing zone, radial cracks, and minor transverse cracks. The failure pattern in Specimen No. 3 was similar to those observed in rocks such as granite [14, 15, 21], sandstone [59, 60], and concrete [10, 12].

Significantly better results were obtained in the tests with the blasting cap. The results were repeatable, and two characteristic zones were distinguished: a crushing zone in the vicinity of the borehole and a fracture zone consisting of radial cracks from the center of the specimen to its edge. The number of radial cracks was similar among the specimens, with four or five visible cracks in each. However, the transverse cracks were less intense than in the specimens subjected to blasting tests with the detonation cord. Some single transversal cracks were observed in Specimens No. 5 and No. 8. Only the blasting cap was considered in subsequent analyses due to the repeatability of the results and more reliable HE parameters. However, future studies of other rock materials should apply the proposed experimental setup to verify the properties of the detonation cord and blasting cap.

Numerical simulation results

Figure 9 presents the blast-induced crack patterns observed within the dolomite specimen for the experimental tests and numerical simulations. The observed cracks in the actual specimens were redrawn based on the photographs to visualize them more clearly. A satisfactory match between the modeling outcomes and actual results was obtained. The average compressive zone in the bottom surface among the four actual specimens was $D_{\text{exp}} = 22.52$ mm. In the numerical model, the diameter of the corresponding zone was $D_{\text{num}} = 23.24$ mm. Material damage due to torquing of the screw bolts and interaction with the steel plates was observed in the outer edge of the FE model of the specimen. Similar phenomena were observed in the real-

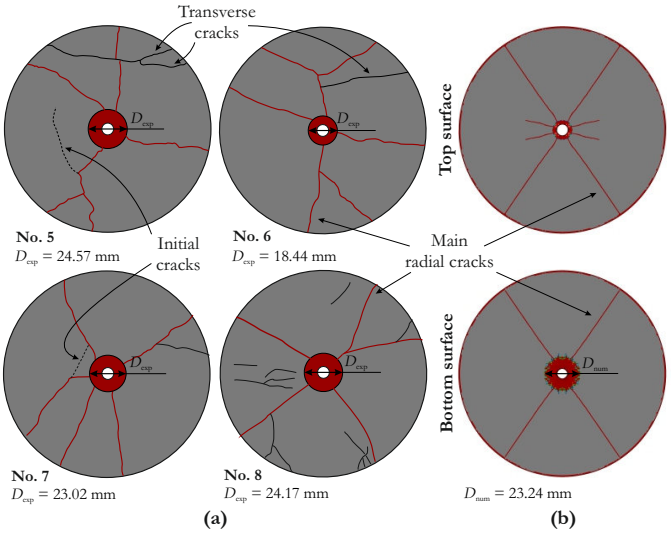

Fig. 9. Comparison of blast-induced crack patterns obtained from (a) experimental tests and (b) numerical simulations

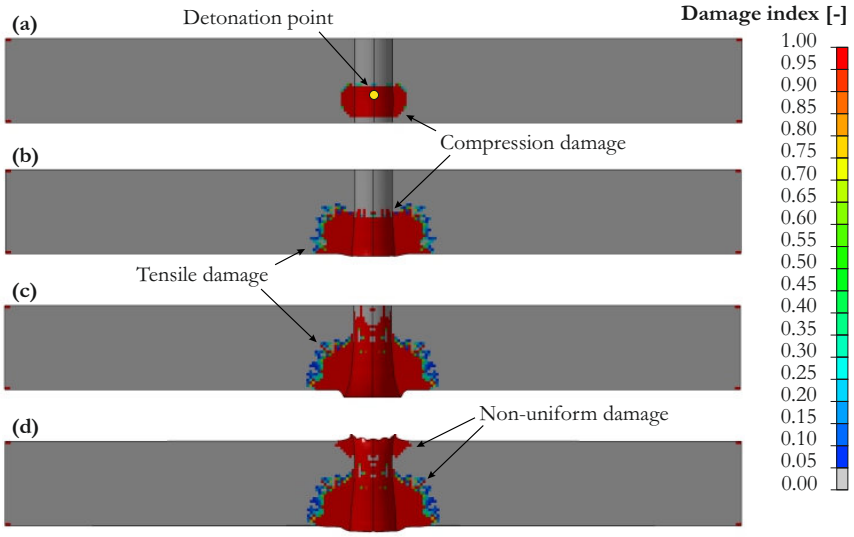

Fig. 10. Side view of the failure process of the dolomite specimen in numerical simulations: (a) $t = 2.5e{-}06$ s, (b) $t = 5.0e{-}06$ s, (c) $t = 1.0e{-}05$ s, (d) $t = 3.0e{-}05$ s

world tests but were more punctate than continuous across the edge. No transverse cracks were observed in the numerical simulations since the model did not consider initial cracks and the real-world properties of the specimen mentioned earlier (heterogeneity, pores, and irregularities).

A side view of the blasting process of the specimen is presented in Fig. 10. The test assumed that plane-strain conditions were met, and therefore identical failure of the specimen in the vicinity of the borehole followed by generation of the crushing zone was expected. However, due to the smaller height of the blasting cap, nonuniform damage across the length of the borehole occurred. Some cracks were also generated perpendicular to the borehole axis because the tensile stress exceeded the tensile strength of the material [61]. These results suggested that a thinner specimen was necessary. However, prior investigations showed that dolomite specimens with a minimum thickness of 7.0 mm were very fragile and fragmented before the blasting tests began. The minimum specimen thickness at which fracture did not occur was 15.0 mm, and therefore this thickness was used in the present study. To determine the appropriate specimen thickness for obtaining uniform damage across the length of the borehole, an additional parametric study using numerical simulations was conducted and is discussed in the next section.

Specimen thickness parametric study

The validated model of the dolomite specimen and experimental setup were used to further analyze the blasting process with specimens of different thicknesses. The main aim of the parametric study was to determine the correct specimen thickness for obtaining uniform compression damage within the borehole length. Several different dimensions were considered, and four selected cases are presented in Fig. 11. At the smallest thickness, which was close to the height of the HE (5.0 mm),

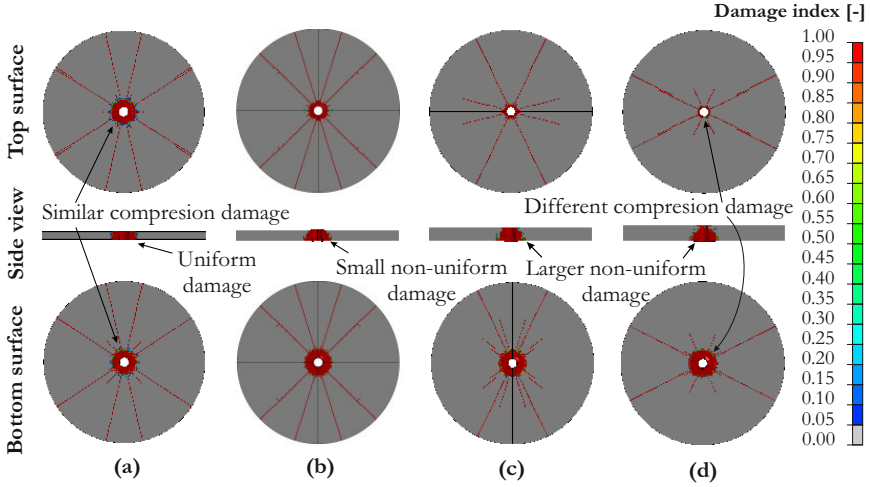

Fig. 11. Comparison of blast-induced crack patterns obtained from numerical simulations of specimens with a thickness of (a) 6.0 mm, (b) 8.0 mm, (c) 10.0 mm, and (d) 12.0 mm

uniform damage across the specimen thickness was observed. Moreover, the cracking patterns in the top and bottom surfaces were identical. These results suggest that HE should be used along the entire length of the borehole to maintain quasi-plane-strain conditions. However, due to the properties of dolomite, it was impossible to prepare and maintain specimens of this thickness for use in experiments. As the specimen thickness increased, the non-uniform damage in the vicinity of the borehole became more pronounced. These differences were largest at thicknesses of 15.0 mm and 12.0 mm, as shown in Figs. 10 and 11, respectively. Eight radial cracks were observed in all cases. However, in the specimens with larger thicknesses, half of the radial cracks were shorter than the others. Ultimately, for the real-world case and the numerical model with a specimen thickness of 15.0 mm, four main radial cracks could be distinguished (see Fig. 9).

To further investigate the influence of specimen thickness, the vertical stress histories were examined. Figures 12 and 13 present the Z-stress histories (stress parallel to the axis of the borehole) for the selected elements across the thickness of the specimen for the models with specimen thicknesses of 6.0 mm and 12.0 mm, respectively. The Z-stress histories were measured from the four elements in the middle of the specimen radius at a distance of approx. 35.0 mm from the borehole center. For the specimen with the smallest thickness, the loading conditions were nearly identical throughout the thickness of the specimen, as evidenced by the measured stress values in all portions of the curves. This corresponds to Fig. 11a, where

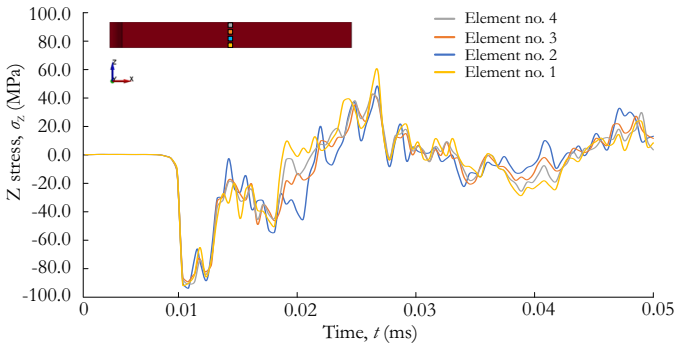

Fig. 12. Comparison of radial stress histories measured for elements along a specimen thickness of 6.0 mm

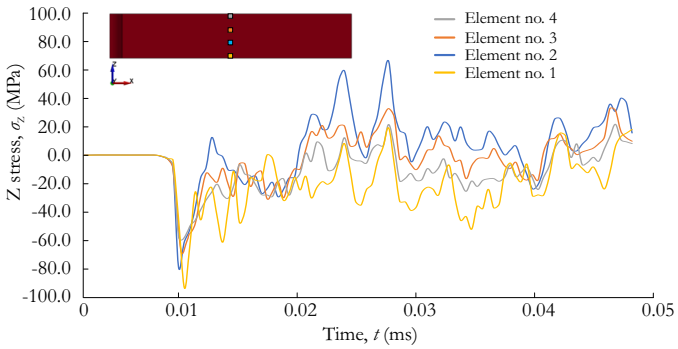

Fig. 13. Comparison of radial stress histories measured for elements along a specimen thickness of 12.0 mm

identical crack patterns on both sides of the specimen and uniform compression damage across the specimen thickness are presented.

By contrast, the loading conditions varied throughout the thicker specimen. In the first peak, different values of minimum stress were observed for each element, i.e., from –61.0 MPa to –93.0 MPa. The first value corresponded to the element on the upper surface of the sample. The stress values decreased from the upper surface to the bottom surface and were the smallest for the element near the bottom surface. The latter portions of the curves did not match until nearly the very end. These outcomes directly correspond to Fig. 11d, where different crack patterns on the bottom and top specimen surfaces can be seen, especially in the case of the compression zone.

6. CONCLUSIONS

The following conclusions can be drawn from the experimental and numerical studies of laboratory blast tests presented here:

- The proposed small-scale blast set-up provides a relatively easy approach to experimental investigation of cracking and subsequent fracturing in rock material induced by blast loading. However, the assumption of plane-strain conditions must be verified for the specific types of materials and detonation sources. In this study, the blasting cap height was too small to maintain uniform compression damage across the length of the borehole. Nevertheless, for the tested configurations, four main radial cracks were observed in the top and bottom surfaces of all specimens, supporting the assumption of quasi-plane strain conditions.
- Due to its heterogeneity and numerous imperfections, inclusions, pores, and initial cracks, the observed cracking characteristics of dolomite differed slightly from those of other rocks, such as granite [14, 15, 21], sandstone [59, 60], and concrete [10, 12]. Nevertheless, typical radial cracks were observed in the bottom and top surfaces of the specimens in the tests using the blasting cap.
- When performing numerical simulations of a blast source inside a tested material, using the correct properties of the HE is crucial. Therefore, special experimental setups were proposed to evaluate the expansion properties of the blasting cap using cylindrical lead specimens and to validate the constants of the JWL EOS. The proposed methods can be effectively used to determine the properties of relatively small HE materials, i.e., detonation cords or blasting caps.
- Following previous works [32,47,49] the ability of the JH-2 material model to reproduce the fracture and fragmentation of dolomite rock was further validated. Consistent with the cited works, satisfactory results were obtained in the present paper. The investigations will be continued and expanded to simulate dolomite behavior in blasting tests, including parallel cut-hole blasting, cracking, and fragmentation.
- The proposed method, which consists of a simple laboratory setup and numerical modeling, can be used to analyze the cracking and fracture of other brittle materials and for the effective validation of parameters of the constitutive models used to capture the behavior of the tested material.

ACKNOWLEDGEMENTS

This research was supported by the Interdisciplinary Centre for Mathematical and Computational Modeling (ICM), University of Warsaw, under grant No. GA73-19. The article was written as part of the implementation of Military University of Technology research grant No 22-876. This support is gratefully acknowledged. The numerical models were prepared using Altair® HyperMesh software.

REFERENCES

[1] H.Y. Shin, P. Thamburaja, A. Srinivasa, and J.N. Reddy, "On simulating impact fracture in high-strength concrete using Gra FEA," *Extrem. Mech. Lett.*, vol. 52, p. 101618, Apr. 2022.

[2] C. Yi, *Improved blasting results with precise initiation: Numerical simulation of small-scale tests and full-scale bench blasting*, Stockholm, 2013.

[3] C. Yi, *Improved blasting results with precise initiation: Numerical simulation of sublevel caving blasting*, Stockholm, 2013.

[4] H. Hu, W. Lu, P. Yan, M. Chen, Q. Gao, and Z. Yang, "A new horizontal rock dam foundation blasting technique with a shock-reflection device arranged at the bottom of vertical borehole," *Eur. J. Environ. Civ. Eng.*, vol. 289, pp. 481-499, Nov. 2017.

[5] Y. Hu, W. Lu, M. Chen, P. Yan, and Y. Zhang, "Numerical simulation of the complete rock blasting response by SPH-DAM-FEM approach," *Simul. Model. Pract. Theory*, vol. 56, pp. 55–68, 2015.

[6] C.P. Yi, P. Zhang, S. Shirzadegan, and U. Nyberg, "Numerical modelling of dynamic response of underground openings under blasting based on field tests," in *Proceedings of the 8th International Symposium on Ground Support in Mining and Underground Construction*, 2016.

[7] X. Huo *et al.*, "Rock damage control for large-diameter-hole lateral blasting excavation based on charge structure optimization," *Tunn. Undergr. Sp. Technol.*, vol. 106, p. 103569, 2020.

[8] W.M. Pytel *et al.*, "Universal approach for risk identification and evaluation in underground facilities," *Min. Sci.*, vol. 27, pp. 165–181, 2020.

[9] W. Pytel, P. Mertuszka, K. Fuławka, A. Lurka, and B. Pałac-Walko, "Resultant axial stresses in instrumented rockbolts induced by dynamic effects occurred due to multi-face blasting in the working areas," *Tunn. Undergr. Sp. Technol.*, vol. 116, p. 104088, 2021.

[10] I. Kukolj, B. Oberdorfer, and F. Ouchterlony, "Internal Fractures After Blasting Confined Rock and Mortar Cylinders," *BHM Berg- und Hüttenmännische Monatshefte*, vol. 164, no. 10, pp. 422–430, 2019.

[11] L.Y. Chi, Z.X. Zhang, A. Aalberg, and C.C. Li, "Experimental Investigation of Blast-Induced Fractures in Rock Cylinders," *Rock Mech. Rock Eng.*, vol. 52, no. 8, pp. 2569–2584, 2019.

[12] I. Kukolj, A. Iravani, and F. Ouchterlony, "Using Small-scale Blast Tests and Numerical Modelling to Trace the Origin of Fines Generated in Blasting," *BHM Berg- und Hüttenmännische Monatshefte*, vol. 163, no. 10, pp. 427–436, 2018.

[13] P.D. Katsabanis, A. Tawadrous, C. Braun, and C. Kennedy, "Timing effects on the fragmentation of small scale blocks of granodiorite," *Fragblast*, vol. 10, no. 1–2, pp. 83–93, Mar. 2006.

[14] M.M. Dehghan Banadaki and B. Mohanty, "Numerical simulation of stress wave induced fractures in rock," *Int. J. Impact Eng.*, vol. 40–41, pp. 16–25, 2012.

[15] S. Gharehdash, M. Barzegar, I.B. Palymskiy, and P.A. Fomin, "Blast induced fracture modelling using smoothed particle hydrodynamics," *Int. J. Impact Eng.*, vol. 135, p. 103235, Jan. 2020.

[16] K. Liu, C. Wu, X. Li, Q. Li, J. Fang, and J. Liu, "A modified HJC model for improved dynamic response of brittle materials under blasting loads," *Comput. Geotech.*, vol. 123, no. December 2019, p. 103584, 2020.

[17] H.Y. Li and G.Y. Shi, "A dynamic material model for rock materials under conditions of high confining pressures and high strain rates," *Int. J. Impact Eng.*, vol. 89, pp. 38–48, 2016.

[18] Z.X. Zhang, D.F. Hou, Z. Guo, and Z. He, "Laboratory experiment of stemming impact on rock fragmentation by a high explosive," *Tunn. Undergr. Sp. Technol.*, vol. 97, p. 103257, 2020.

[19] Z. Wang, H. Wang, J. Wang, and N. Tian, "Finite element analyses of constitutive models performance in the simulation of blast-induced rock cracks," *Comput. Geotech.*, vol. 135, p. 104172, Jul. 2021.

[20] J. Tao, X.G. Yang, H.T. Li, J.W. Zhou, S.C. Qi, and G. Da Lu, "Numerical investigation of blast-induced rock fragmentation," *Comput. Geotech.*, vol. 128, p. 103846, 2020.

[21] L.X. Xie *et al.*, "JHR constitutive model for rock under dynamic loads," *Comput. Geotech.*, vol. 108, pp. 161–172, 2019.

[22] Z. Zhu, B. Mohanty, and H. Xie, "Numerical investigation of blasting-induced crack initiation and propagation in rocks," *Int. J. Rock Mech. Min. Sci.*, vol. 44, no. 3, pp. 412–424, 2007.

[23] W. Wilson and D.C. Holloway, "Fragmentation Studies In Instrumented Concrete Models," in *6th ISRM Congress*, 1987.

[24] J.E. Field and A. Ladegaard-Pedersen, "The importance of the reflected stress wave in rock blasting," *Int. J. Rock Mech. Min. Sci.*, vol. 8, no. 3, pp. 213–226, 1971.

[25] H. Jeong, B. Jeon, S. Choi, and S. Jeon, "Fracturing behavior around a blasthole in a brittle material under blasting loading," *Int. J. Impact Eng.*, vol. 140, p. 103562, 2020.

[26] F. Zhu and J. Zhao, "Peridynamic modelling of blasting induced rock fractures," *J. Mech. Phys. Solids*, vol. 153, p. 104469, 2021.

[27] J. Wang, Y. Yin, and K. Esmaieli, "Numerical simulations of rock blasting damage based on laboratory-scale experiments," *J. Geophys. Eng.*, vol. 15, no. 6, pp. 2399–2417, Aug. 2018.

[28] J. Wang, Y. Yin, and C. Luo, "Johnson–Holmquist-II(JH-2) Constitutive Model for Rock Materials: Parameter Determination and Application in Tunnel Smooth Blasting," *Appl. Sci.*, vol. 8, no. 9, p. 1675, Sep. 2018.

[29] T.J. Holmquist, G.R. Johnson, D.E. Grady, C.M. Lopatin, and E.S. Hertel, "High strain rate properties and constitutive modeling of glass," in *Proceedings of 15th International Symposium on Ballistics*, 1995, pp. 234–244.

[30] T.J. Holmquist, D.W. Templeton, and K.D. Bishnoi, "Constitutive modeling of aluminum nitride for large strain, high-strain rate, and high-pressure applications," *Int. J. Impact Eng.*, vol. 25, no. 3, pp. 211–231, 2001.

[31] G.R. Johnson and T.J. Holmquist, "An improved computational constitutive model for brittle materials," *AIP Conf. Proc.*, vol. 309, no. 1, pp. 981–984, 1994.

[32] P. Baranowski *et al.*, "Fracture and fragmentation of dolomite rock using the JH-2 constitutive model: Parameter determination, experiments and simulations," *Int. J. Impact Eng.*, vol. 140, p. 103543, 2020.

[33] A. Kurzawa, D. Pyka, J. Pach, K. Jamroziak, and M. Bocian, "Numerical Modeling of the Microstructure of Ceramic-Metallic Materials," *Procedia Eng.*, vol. 199, pp. 1495–1500, 2017.

[34] P. Kędzierski, A. Morka, G. Sławiński, and T. Niezgoda, "Optimization of two-component armour," *Bull. Polish Acad. Sci. Tech. Sci.*, vol. 63, no. 1, pp. 173–179, 2015.

[35] G.M. Ren, H. Wu, Q. Fang, and X.Z. Kong, "Parameters of Holmquist–Johnson–Cook model for high-strength concrete-like materials under projectile impact," *Int. J. Prot. Struct.*, vol. 8, no. 3, pp. 352–367, 2017.

[36] T.J. Holmquist, G.R. Johnson, and W.H. Cook, "A computational constitutive model for concrete subjected to large strains, high strain rates, and high pressures," in *The 14th international symposium on ballistic*, 1993, pp. 591–600.

[37] M. Kucewicz, P. Baranowski, and J. Małachowski, "Dolomite fracture modeling using the Johnson–Holmquist concrete material model: Parameter determination and validation," *J. Rock Mech. Geotech. Eng.*, vol. 13, no. 2, pp. 335–350, 2021. doi: 10.1016/j.jrmge.2020.09.007.

[38] M. Pająk, P. Baranowski, J. Janiszewski, M. Kucewicz, Ł. Mazurkiewicz, and B. Łaźniewska-Piekarczyk, "Experimental testing and 3D meso-scale numerical simulations of SCC subjected to high compression strain rates," *Constr. Build. Mater.*, vol. 302, p. 124379, 2021.

[39] L. Mazurkiewicz, J. Małachowski, P. Baranowski, K. Damaziak, W. Pytel, and P. Mertuszka, "Numerical modelling of detonation in mining face cut-holes," in *Advances in Mechanics: Theoretical, Computational and Interdisciplinary Issues – 3rd Polish Congress of Mechanics, PCM 2015 and 21st International Conference on Computer Methods in Mechanics, CMM 2015*, 2016, pp. 393–396.

[40] C. Yi, J. Sjöberg, and D. Johansson, "Numerical modelling for blast-induced fragmentation in sublevel caving mines," *Tunn. Undergr. Sp. Technol.*, vol. 68, pp. 167–173, Sep. 2017.

[41] L.E. Schwer and Y.D. Murray, "Continuous Surface Cap Model for Geomaterial Modeling: A New LS-DYNA Material Type," *7 th International LS-DYNA Users Conference, Material Technology (2)*, 2022.

[42] G. Morales-Alonso, J. Magnusson, H. Hansson, A. Ansell, F. Gálvez, and V. Sánchez-Gálvez, "Behaviour of concrete structural members subjected to air blast loading," in *Proceedings – 27th International Symposium on Ballistics, BALLISTICS 2013*, 2013, vol. 1, pp. 936–947.

[43] M. Kucewicz, P. Baranowski, and J. Małachowski, "Determination and validation of Karagozian-Case Concrete constitutive model parameters for numerical modeling of dolomite rock," *Int. J. Rock Mech. Min. Sci.*, vol. 129, p. 104302, 2020.

[44] A. Mardalizad, R. Scazzosi, A. Manes, and M. Giglio, "Testing and numerical simulation of a medium strength rock material under unconfined compression loading," *J. Rock Mech. Geotech. Eng.*, vol. 10, no. 2, pp. 197–211, 2018.

[45] L.J. Malvar, J.E. Crawford, J.W. Wesevich, and D. Simons, "A plasticity concrete material model for DYNA3D," *Int. J. Impact Eng.*, vol. 19, no. 9, pp. 847–873, 1997.

[46] P. Baranowski, M. Kucewicz, J. Małachowski, and P.W. Sielicki, "Failure behavior of a concrete slab perforated by a deformable bullet," *Eng. Struct.*, vol. 245, p. 112832, 2021. doi: 10.1016/j.engstruct. 2021.112832.

[47] P. Baranowski, Ł. Mazurkiewicz, J. Małachowski, and M. Pytlik, "Experimental testing and numerical simulations of blast-induced fracture of dolomite rock," *Meccanica*, vol. 55, no. 12, pp. 2337–2352, 2020.

[48] D. Xiao, Z. Zhu, R. Hu, and L. Lang, "Study of testing method for dynamic initiation toughness of sandstone under blasting loading," *Shock Vib.*, vol. 2018, p. 1043298, 2018.

[49] P. Baranowski, M. Kucewicz, M. Pytlik, and J. Małachowski, "Shock-induced fracture of dolomite rock in small-scale blast tests," *J. Rock Mech. Geotech. Eng.*, 2022, doi: 10.1016/j.jrmge.2021.12.022.

[50] J. Hallquist, *LS-DYNA Theory Manual*, vol. 19. Livermore Software Technology Corporation (LSTC), 2019.

[51] R. Grzejda, "Finite element modeling of the contact of elements preloaded with a bolt and externally loaded with any force," *J. Comput. Appl. Math.*, vol. 393, p. 113534, 2021.

[52] K. Puchała, E. Szymczyk, J. Jachimowicz, P. Bogusz, and M. Sałaciński, "The influence of selected local phenomena in CFRP laminate on global characteristics of bolted joints," *Materials (Basel).*, vol. 12, no. 24, pp. 4139, 2019.

[53] A. Kurzawa *et al.*, "Assessment of the impact resistance of a composite material with EN AW-7075 matrix reinforced with α-Al2O3 particles using a 7.62 $\times$ 39 mm projectile," *Materials (Basel)*, vol. 13, no. 3, p. 769, 2020.

[54] M. Kucewicz, P. Baranowski, J. Małachowski, W. Trzciński, and L. Szymańczyk, "Numerical Modelling of Cylindrical Test for Determining Jones – Wilkins–Lee Equation Parameters," in *Proceedings of the 14th International Scientific Conference: Computer Aided Engineering*, 2019, pp. 388–394.

[55] G.R. Johnson and W.H. Cook, "A constitutive model and data for metals subjected to large strains, high strain rates and high temperatures," in *Proceedings 7th International Symposium on Ballistics*, 1983, pp. 541–547.

[56] P. Baranowski, R. Gieleta, J. Malachowski, K. Damaziak, and L. Mazurkiewicz, "Split Hopkinson Pressure Bar impulse experimental measurement with numerical validation," *Metrol. Meas. Syst.*, vol. 21, no. 1, pp. 47–58, 2014.

[57] P. Kędzierski, A. Morka, S. Stanisławek, and Z. Surma, "Numerical modeling of the large strain problem in the case of mushrooming projectiles," *Int. J. Impact Eng.*, vol. 135, p. 103403, 2019.

[58] T. Břrvik, S. Dey, and A.H. Clausen, "Perforation resistance of five different high-strength steel plates subjected to small-arms projectiles," *Int. J. Impact Eng.*, vol. 36, no. 7, pp. 948–964, Jul. 2009.

[59] X. Wang, Z. Zhu, M. Wang, P. Ying, L. Zhou, and Y. Dong, "Study of rock dynamic fracture toughness by using VB-SCSC specimens under medium-low speed impacts," *Eng. Fract. Mech.*, vol. 181, pp. 52–64, 2017.

[60] L. Yu, H. Su, H. Jing, Q. Zhang, and E. Yang, "Experimental study of the mechanical behavior of sandstone affected by blasting," *Int. J. Rock Mech. Min. Sci.*, vol. 93, pp. 234–241, 2017.

[61] C. Zou, J. Li, X. Zhao, and J. Zhao, "Why are tensile cracks suppressed under dynamic loading? – Transition strain rate for failure mode," *Extrem. Mech. Lett.*, vol. 49, p. 101506, Nov. 2021.